JCAMECH

*Vol. 50, No. 2, December 2019, pp 228-238*
*DOI: 10.22059/jcamech.2018.243247.193*

# Modelling of the Dynamics of an immersed body in a microchannel with stenosis using the immersed boundary method

*Ali Falavand Jozaei[a,*], Asad Alizadeh[a] , and Ashkan Ghafouri[a]*

[a] *Department of Mechanical Engineering, Ahvaz Branch, Islamic Azad University, Ahvaz, Iran*

ARTICLE INFO

*Article history:*
Received: 02 November 2017
Accepted: 02 January 2018

*Keywords:*
Flexibility
Stenosis
Poiseuille Flow
Lattice Boltzmann Method
Immersed Boundary Method

ABSTRACT

In the present study, the combination of lattice Boltzmann and immersed boundary methods is used to simulate the motion and deformation of a flexible body. Deformation of the body is studied in microchannel with stenosis and the effect of the flexibility changes on its deformation is investigated. The obtained results in the present manuscript show that by increasing the elasticity modulus, the deformation of the body and its speed decrease. In this case, the flow pressure around the body increase. When the body is initially located outside the microchannel center, tank-treading motion occurs due to the difference in velocity of the shear layers. In addition, with a decrease in the size of microchannel stenosis, the body is less deformed and goes faster and reaches to the end of the microchannel in less time. The faster or slower movement of the biological membranes than the normal state causes the proper exchange of materials between the membrane wall and the surrounding flow and that disturbs its most important duty i.e. the exchange of materials with tissues. The analysis in this study shows that the results of the simulation are in good agreement with the available results and demonstrates the efficiency of the combination of lattice Boltzmann and immersed boundary methods to simulate the dynamic behavior of biological membranes, red blood cells and deformable particles inside the flow.

## 1. Introduction

Fluid-structure interaction (FSI) problems are of great important in fluid dynamics[1]. It is also used in biomechanics problems [2,3]. The immersed boundary method (IBM) is the most appropriate approach for solving such problems taking the advantage of a fixed uniform computational grid [4,5]. Therefore, the IBM can be easily used to simulate the medical and pharmaceutical contexts including red blood cells motion, and blood flow in vessels and heart valves. IBM is both a mathematical formulation and a numerical scheme. The mathematical formulation uses a combination of Eulerian and Lagrangian parameters. Theses parameters are linked together via interaction equations where the Dirac delta function plays an important role. In numerical implementation of IBM, the Eulerian variables are defined on a fixed Cartesian grid and the Lagrangian variables are defined on a curvilinear grid moving freely through the Eulerian grid. The basis of IBM is to add a forcing term as a source term to the Navier-Stokes or lattice Boltzmann equations [6]. In recent years, the lattice Boltzmann method (LBM) has developed into a promising numerical method for the simulation of complex fluid flows. Unlike conventional numerical schemes, which are based on discretization of macroscopic continuum equations, the LBM is based on microscopic models and mesoscopic kinetic equations. The LBM is a reliable alternative to the conventional computational fluid dynamics methods for the simulation of complex problems including incompressible fluid flows, porous media flows, multi-phase flows and blood flow. When Mach number and Knudsen number are small enough, the LBM equation is a good approximation for Navier-Stokes (N-S) equations. In LBM, fluid is considered as a combination of virtual particles, which can move in a finite number of directions. This method comprises two steps: streaming and collision. In the streaming step, the particles move to the neighbor body lattice points. In the collision step, the particles arriving at the points, interact one another and change their velocity directions according to scattering rules. LBM has been found to recover the N-S equation using Chapman-Enskog expansion [7]. The most important features of the LBM are: explicit updating, algebraic operation and easy implementation on curved boundaries. There have been many researchers who have combined the IBM-LBM to solve the fluid flows involving rigid/elastic interfaces. Feng and Michaelides [8] were the first to combine the LBM with the IBM and simulated suspensions of rigid disks in 2D. Le and Zhang [9] used in their work a hybrid LBM-IBM and noticed that the computed velocity profiles can deviate greatly from theoretical ones even for very simple flow situations, both in the immersed boundary layer and the bulk region. Dupuis et al. [10] studied how the coupling method of the forcing term between the Eulerian and Lagrangian grids could affect the results for the flow over an impulsively started cylinder at moderate Reynolds (Re) number.Wu and Shu

* Corresponding author. Tel.: +98-91-6610-3732; fax: + 98-61-3334-8356; e-mail: falavand@iauahvaz.ac.ir

[11] proposed a new version of IBM-LBM, which could well consider the effect of external force on the momentum flux as well as the discrete lattice effect. JiSeok and SangHwan [12] presented a numerical scheme for fluid-structure interaction, especially for elastic structures. They employed a hybrid LBM-IBM using an improved direct forcing scheme for the fluid, and a finite element method with Euler beam elements for the elastic plate. Zhang et al. [13, 14] also used a combination of the IBM and the LBM to investigate the microscopic hemodynamic and hemorheological behaviors of discrete RBCs in shear flow. They noted that three-dimensional simulation of RBCs is required to attain accurate results. Cheng et al. [15] proposed a model to properly simulate the fast boundary movements and steep pressure gradient occurring in the fluid–body interaction. They simulated the mitral valve jet flow considering the interaction of leaflets and fluid. The combination of the Lattice-Boltzmann and the immersed boundary method has been used extensively in recent years in modeling biomechanics problems [16-19]. Recently, this method has been used to simulate the flow around rigid bodies [20-22], and to simulate the motion and deformation of the flexible membrane (fluid-structure interaction problem) [23-26]. Also recently, Boltzmann's method has been used for multiphase flows [27-31], non- Newtonian fluid [32] and solution of differential equations [33,34].

In the present work, the effect of elastic modulus changing and the initial location of the membrane and increasing the microchannel stenosis diameter on the dynamic behavior of the flexible boundary are investigated using combination of lattice Boltzmann and the immersed boundary methods.

## 2. Mathematical formulations

The discretized LBM equation is written in the form of Eq. (1).

$$f_i(\vec{x}+\hat{e}_i\Delta t, t+\Delta t)-f_i(\vec{x},t) = -\frac{f_i(\vec{x},t)-f_i^{eq}(\vec{x},t)}{\tau}+\Delta t\, S_i \tag{1}$$

where $f_i(\vec{x},t)$ is the density distribution function of a particle with speed $\hat{e}_i$ located at position $\vec{x}$ at time $t$. $\Delta t$ is the time step, $f_i^{eq}(\vec{x},t)$ is the equilibrium distribution function, $\tau$ indicates the relaxation time and $S_i$ is the body force of the immersed body in the LBM equation. It should be noted that, the LBM equation can recover the N-S equations by the so-called Chapman-Enskog expansion. The velocities of the particles can be written in the form of Eq. (2):

$$\hat{e}_i = \begin{cases} (i,i) & ; i=0 \\ (\cos\frac{\pi}{2}(i-1), \sin\frac{\pi}{2}(i-1))c & ; i=1-4 \\ \sqrt{2}(\cos\frac{\pi}{2}(i-\frac{9}{2}), \sin\frac{\pi}{2}(i-\frac{9}{2}))c & ; i=5-8 \end{cases} \tag{2}$$

In Eq. (2), $c=\Delta x/\Delta t$ and $\Delta x$ is the distance between two adjacent nodes in the Eulerian grid. The equilibrium distribution function defined as follows,

$$f_i^{eq}(\vec{x},t) = w_i\rho\left[1+3\frac{(\hat{e}_i.\vec{u})}{c^2}+\frac{9}{2}\frac{(\hat{e}_i.\vec{u})^2}{c^4}-\frac{3}{2}\frac{|\vec{u}|^2}{c^2}\right] \tag{3}$$

where $w_i$ is the weight coefficients given by,

$$w_i = \begin{cases} \frac{4}{9} & ; i=0 \\ \frac{1}{9} & ; i=1-4 \\ \frac{1}{36} & ; i=5-8 \end{cases} \tag{4}$$

However, the elastic force in LBM is defined as Eq. (5),

$$S_i = (1-\frac{1}{2\tau})w_i\left[\frac{3(\hat{e}_i-\vec{u})}{c^2}+\frac{9(\hat{e}_i.\vec{u})}{c^4}\hat{e}_i\right].\vec{f} \tag{5}$$

Macroscopic fluid density is obtained by the following relation,

$$\rho = \sum_{i=0}^{8} f_i \tag{6}$$

In addition, the macroscopic velocity field $\vec{u}$ is defined as:

$$\vec{u} = \frac{1}{\rho}\left[\sum_{i=0}^{8} f_i\,\hat{e}_i + \frac{1}{2}\vec{f}\,\Delta t\right] \tag{7}$$

The Lagrangian force density $\vec{L}$ comprises two components of stretching/compression force $\vec{L}_s$ and bending force $\vec{L}_b$ defined as [23]:

$$\vec{L}(s,t) = \vec{L}_s(s,t)+\vec{L}_b(s,t) \tag{8}$$

The Lagrangian force density is related to the elastic energy density using the virtual work theorem:

$$\vec{L}(s,t) = -\frac{\partial £}{\partial\vec{X}} = -\frac{\partial(£_s+£_b)}{\partial\vec{X}} \tag{9}$$

Therefore, the elastic energy density consists of stretching/compression $£_s$ and bending $£_b$ components, which are given in discretized form as:

$$£_s = \frac{1}{2}E_s\sum_{j=1}^{N-1}\left(\frac{|\vec{X}_{j+1}-\vec{X}_j|}{\Delta s}-1\right)^2\Delta s \tag{10}$$

$$£_b = \frac{1}{2}E_b\sum_{j=2}^{N-1}\left(\frac{|\vec{X}_{j+1}-2\vec{X}_j+\vec{X}_{j-1}|^2}{(\Delta s)^4}\right)\Delta s \tag{11}$$

The discretized form of the Lagrangian force density components is given by the following relations:

$$(\vec{L}_s)_k = \frac{E_s}{(\Delta s)^2}\sum_{j=1}^{N-1}\left\{\begin{array}{l}(|\vec{X}_{j+1}-\vec{X}_j|-\Delta s)\times \\ \frac{\vec{X}_{j+1}-\vec{X}_j}{|\vec{X}_{j+1}-\vec{X}_j|}(\delta_{j,k}-\delta_{j+1,k})\end{array}\right\} \tag{12}$$

$$(\vec{L}_b)_k = \frac{E_b}{(\Delta s)^4}\sum_{j=2}^{N-1}\begin{Bmatrix}(\vec{X}_{j+1} - 2\vec{X}_j + \vec{X}_{j-1}) \\ (2\,\delta_{j,k} - \delta_{j+1,k} - \delta_{j-1,k})\end{Bmatrix} \tag{13}$$

In Eqs. (10) to (13), $k = 1,2,\dots,N$ ($N$ is the total number of Lagrangian nodes on the body), $(\vec{L}_s)_k$ and $(\vec{L}_b)_k$ are Lagrangian force density components associated with the node $k$ on the body and $\delta_{j,k}$ is the Kronecker delta function. Interaction between the fluid and body can be achieved by obtaining a proper relationship between the Lagrangian parameters associated with the cell and Eulerian parameters associated with the fluid. In this section, it is shown how to transfer the Lagrangian force to the Eulerian frame and also how to interpolate velocities from Eulerian to Lagrangian coordinates. The Eulerian force density $\vec{f}(\vec{x},t)$ is obtained by integrating the Lagrangian force density $\vec{L}(s,t)$ :

$$\vec{f}(\vec{x},t) = \int_{\Gamma} \vec{L}(s,t)\,\delta(\vec{x} - \vec{X}(s,t))ds \tag{14}$$

where $\Gamma$ represents the immersed elastic boundary and $\delta\left(\vec{x} - \vec{X}(s,t)\right)$ is the Dirac delta function.

To enforce the no-slip condition on the fluid-body interface, the velocity of the body wall should be set equal to the adjacent fluid velocity, i.e.,

$$\vec{U}(s,t) = \vec{u}(\vec{X}(s,t),t) = \frac{\partial \vec{X}(s,t)}{\partial t} = \int_{\Gamma} \vec{u}(\vec{x},t)\;\delta(\vec{x} - \vec{X}(s,t))\;dx \tag{15}$$

It should be noted that in the present work, the fluid velocity $\vec{u}(\vec{x},t)$ is obtained using the LBM.

Mathematically the Dirac delta function $\delta(\vec{x})$ is discontinuous and has to be smoothed for numerical implementation. There are different methods of smoothing this function. The following smoothed delta function is proposed by [6]:

$$\delta(\vec{x}) = \frac{1}{h^2}\,\phi(\frac{x}{h})\,\phi(\frac{y}{h})$$
$$\phi(r) = \begin{Bmatrix}\frac{1}{4}(1+\cos\frac{\pi r}{2}) & ; & |r| \le 2 \\ 0 & ; & |r| > 2\end{Bmatrix} \tag{16}$$

where $h$ is the distance between two Eulerian grid points and $r$ denotes the distance between any two Eulerian and Lagrangian points.

**3. Results**

*3.1. Validation*

In this section, the motion of a circular elastic body in shear flow is studied. Length and width of the microchannel is considered to be 16 times of the original radius of the body. The body is positioned at the center of microchannel and 160 Lagrangian points have been used. In Fig.1a, capsule deformation and tank-treading movement are observed. where G and $E_B$ are 0.04 and 0-0.4 respectively. which are calculated by the equations $G = \frac{\mu k a}{E_s}$ and $E_B = \frac{E_b}{a^2 E_s}$. G is dimensionless shear rate, k is shear rate (1/s), a is initial capsule radius, $E_s$ is elastic modulus (N/m), $E_b$ is bending modulus (N.m) and $E_B$ is dimensionless bending modulus. Taylor deformation parameter is defined as $D_{xy} = \frac{L-B}{L+B}$. In Fig. 1b, the introduced variables are shown. By increasing the bending modulus, the deformation of the body decreased. In Figs.1c and 1d present results have been compared with Sui and et.al [35] results. By increasing bending modulus, Taylor deformation parameter is decreased, which represents less deformation of capsule. In addition, it can be seen from Fig. 1 (d), by decreasing bending modulus, dimensionless angle $\frac{\theta}{\pi}$ is decreased. The result that is obtained from this section is that: by decreasing bending modulus, deformation of body increased and orientation of the body to the horizon decreased and its shape becomes oblique. In fact, the circle has become ellipse, and with the further decreasing of the bending modulus, the ellipse becomes more elongated. Present results are in good agreement with Sui et al. [35] results.

*3.2. The behavior of a flexible body in passing through stenosis*

A circular body with a diameter of H=30 µm is considered in the poiseuille flow. Length and height of microchannel are L= 300 µm and D= 60 µm and in stenosis section (half oval in the middle of microchannel) is d= 20 µm (d/D=1/3). Reynolds number is Re= 0.5 (Fig. 2). The bounce-back and periodic boundary conditions have been used on the walls and on the inlet and exit of the microchannel and the boundary condition BFL has applied on curvilinear boundaries [36]. First, the dynamics of the circular body which located at the center of the microchannel, in two case of high and low flexibility are examined with elastic and bending $14\times10^{-19}$ N.m, $1\times10^{-19}$ N.m and $5\times10^{-5}$ N.m, $19\times10^{-19}$ N.m respectively.

In Figs. 3 and 4, motion of the body, with high and low flexibilities at different times, is observed while passing the stenosis. Pressure is considered in grid unit. One can see in Fig. 3 that body with high flexibility is stretched more and reaches the end of microchannels in less time. The low-flexible body (Fig.4), reduces somewhat the effective cross-sectional area of the fluid behind the body due to its high hardness. In fact, it is similar to blocking a greater amount of flow path (relative to the body with high flexibility), which reduces the flow velocity behind the body and increases the flow pressure behind the immersed body according to Figs. 3b and 4b. In both cases, since the boundary is located in the center of the microchannel and the axial flow is symmetrical, a balance is occurred between the upper and lower lift forces acting on the body. Thus, the body is not displaced vertically. The difference in pressure created behind and in front of the body causes it to move in the longitudinal direction of the microchannel. The greater pressure on the back side relative to front, makes the rear side form concave shape, while the front is stretched more and in after. Therefore, it’s shape become convex before stenosis.

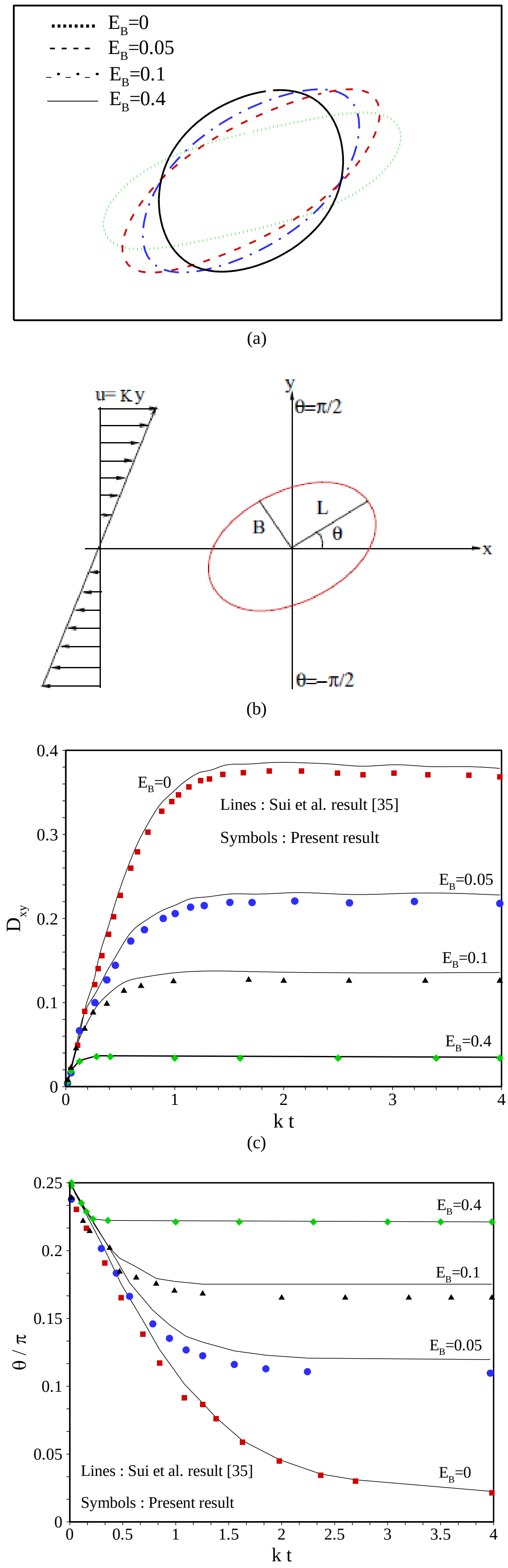


**Figure 1.** a) The effect of bending modulus on deformation of circular body (present result) ; b) represent L, B, θ; c) Taylor deformation parameter changes for

different times; d) θ/π change for different times.

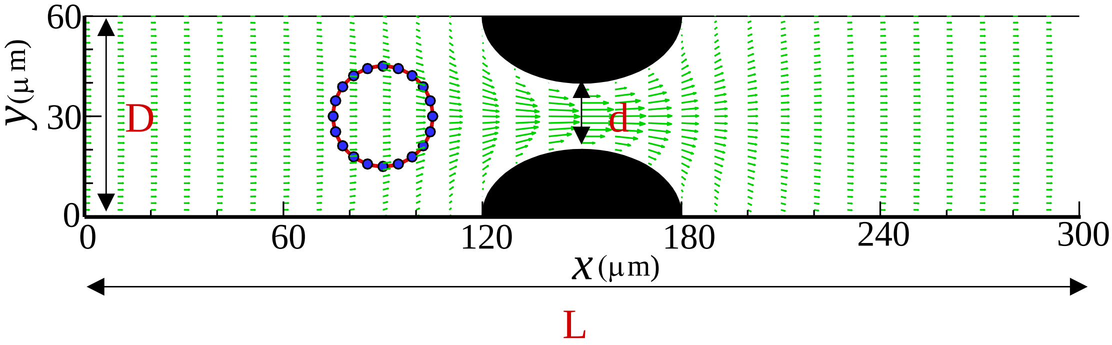


**Figure 2:** The initial position of the immersed body located at the center of the microchannel

Figure 5 shows that a body with a high elasticity modulus has a lower rate of velocity than the body with a low elastic modulus. This matter is also observed in the results of others researches [37, 38]. It should be noted that the acceleration or deceleration movement of biological membranes than the normal state, results in the lack of proper exchange of materials between the membrane wall and the surrounding flow and interferes with its most important task, ie, the exchange of materials with tissues. The body with high flexibility, reaches the end of the microchannel at a shorter time due to its faster velocity. In both cases, the body appears to be faster when it comes to stenosis due to increased flow velocity in this area.

Figure 6 shows that the A/B ratio is higher for more deformable body due to its low elasticity modulus. When the immersed body reaches to stenosis, it is most deformed due to the increase in speed in this area. In this case, the body in the moment of passing thorough stenosis is more stretched and passes through the stenosis more easily with less energy from the fluid. After exiting from stenosis, the body reaches convex at front and reaches concave at behind it (Fig. 3d) due to its high flexibility. While the body with low deformability, maintains its circular shape after exiting from stenosis.

In Fig. 7, the initial location of the body is placed under the center of the microchannel. The body's rotation (tank-treading) is caused by the shear force of the fluid around it. Due to the rotational phenomenon, a lifting force is applied to the deformed membrane and directs it towards the center of the microchannel. In the rotational movement, after a change in the initial shape, the shape and the movement direction of the body remain constant during the movement (after the stenosis); because the flow inside the microchannel is viscous, so it has shear layers. The shear is caused by horizontal component of the fluid velocity. It means that, the velocity in the vertical axis varies within the shear layers. Therefore, when fluid collides to the boundary, the upper part of the boundary is affected by higher velocity than the lower part. This difference in momentum on the body causes it to rotate. As a result of this rotation, an upward lift force from the fluid to the body is applied and directs it to the center of the microchannel.

In this case, the maximum deformation of the body is observed when it passes through the stenosis. The body with high elasticity (Fig. 7a) is more stretched when passing through the stenosis compared to the body with low elasticity (Fig. 7b), while the body with low elasticity blocks a greater pass of flow that reduces the velocity and increases the pressure around the body. The red solid points are related to the rotation of the body (tank-treading movement). This type of motion has been observed in the experimental and numerical results [39-41]. In Figs. 7c and 7d, the velocity vector of Lagrangian points of immersed body with high and low elasticity are observed at the exit of stenosis. The body with high elasticity adapts itself to the flow path and passes stenosis with less energy. A body with low elasticity blocks the outlet span of stenosis for a moment. The velocity vector of the Lagrangian points in comparison to the previous one cannot easily fit itself with the streamline. In this case, a higher pressure is applied to the back of the body so that the flow can pass the body from the stenosis. This behavior of body in the passing the stenosis leads to slowing down its motion.

Figure 8 shows the effects of decreasing the height of the stenosis for the body with low flexibility (Fig. 4). Figure 8a shows deformation of body with low flexible for case d/D = 2/3. Reducing the stenosis causes reduction in the deformability of the body. The body has the least deformation in the case without stenosis (Figure 8b). It is seen from the Figure 8c that the velocity of the body increases with decreasing stenosis height. By creating stenosis, the loss due to obstruction increases and as a result, the body velocity decreases. Stenosis causes the body to slow down before and after the stenosis and increases its velocity value when crossing the stenosis.

## 4. Conclusion

In the present study, the combination of the lattice Boltzman method and the immersed boundary method was used to simulate the motion and deformation of a flexible body in a viscous flow. By increasing the elasticity modulus, the deformation and velocity of the body decreased. In this case, the pressure of the flow around the body increasesd. In addition, by decreasing the size of stenosis of the microchannel, the body was less deformed and had higher velocity, resulting in less time to reach at the end of microchannel. Also, the results of the simulation were in good agreement with the available results. By performing this numerical study and study of a number of different parameters, one can study the physics of flow and the effect of solid and fluid interaction on each other. Each individual behavior of these parameters gives the reader a view that does not feel the vacuum of experimental works in this field. Investigating various parameters affecting fluid flow and immersed membrane helps to understand biological systems.It is also possible to observe the lattice Boltzmann-immersed boundary method’s ability to model the dynamic behavior of biological membranes, red blood cells, and other deformable particles in the flow and compare the simplicity of programming and convergence rate of this method with other CFD methods.

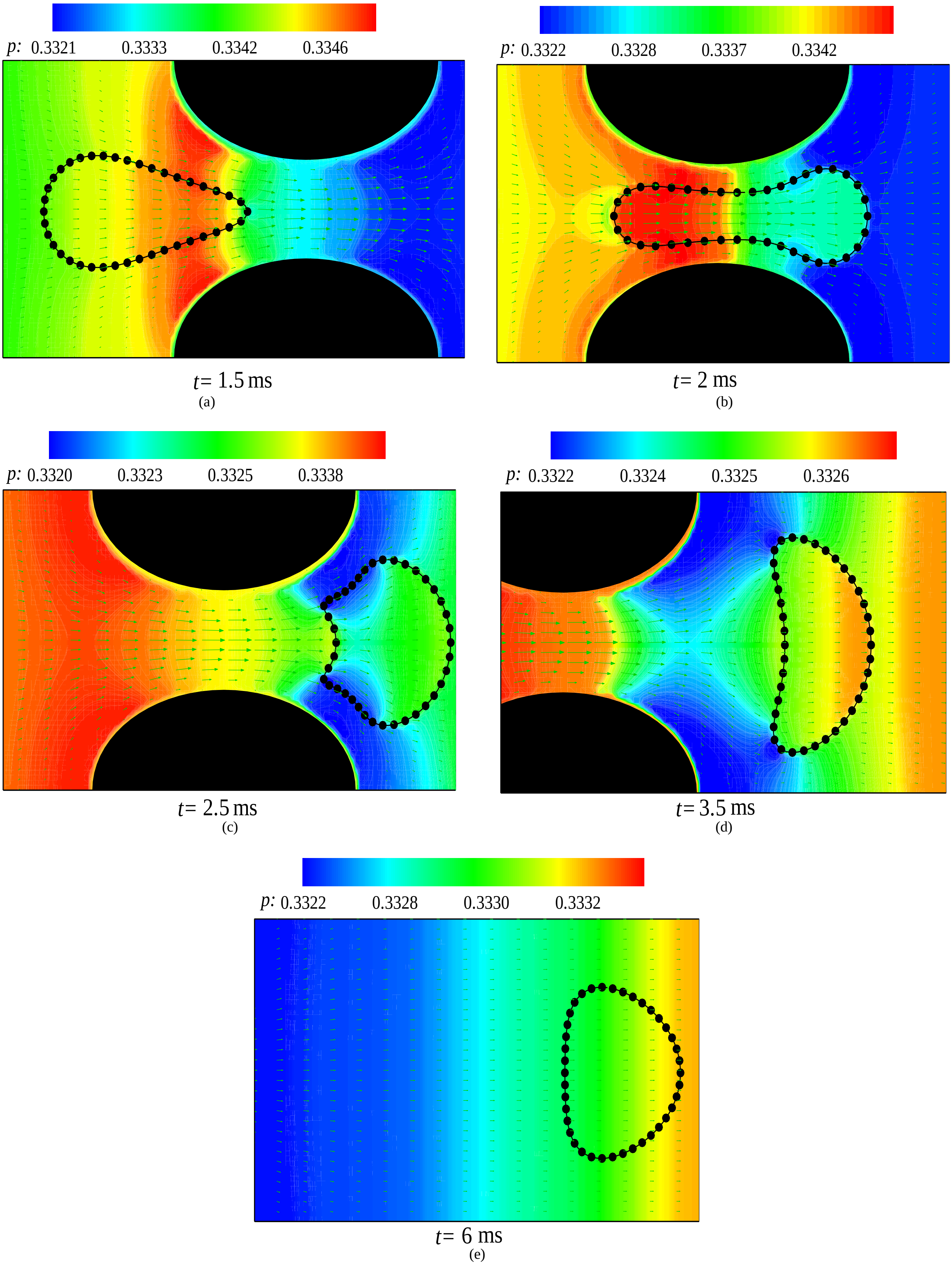


**Figure 3.** Motion of the body with a high flexibility passing stenosis at the times a) t = 1.5ms, b) t = 2ms, c) t = 2.5ms, d) t = 3.5ms and e) t = 6ms

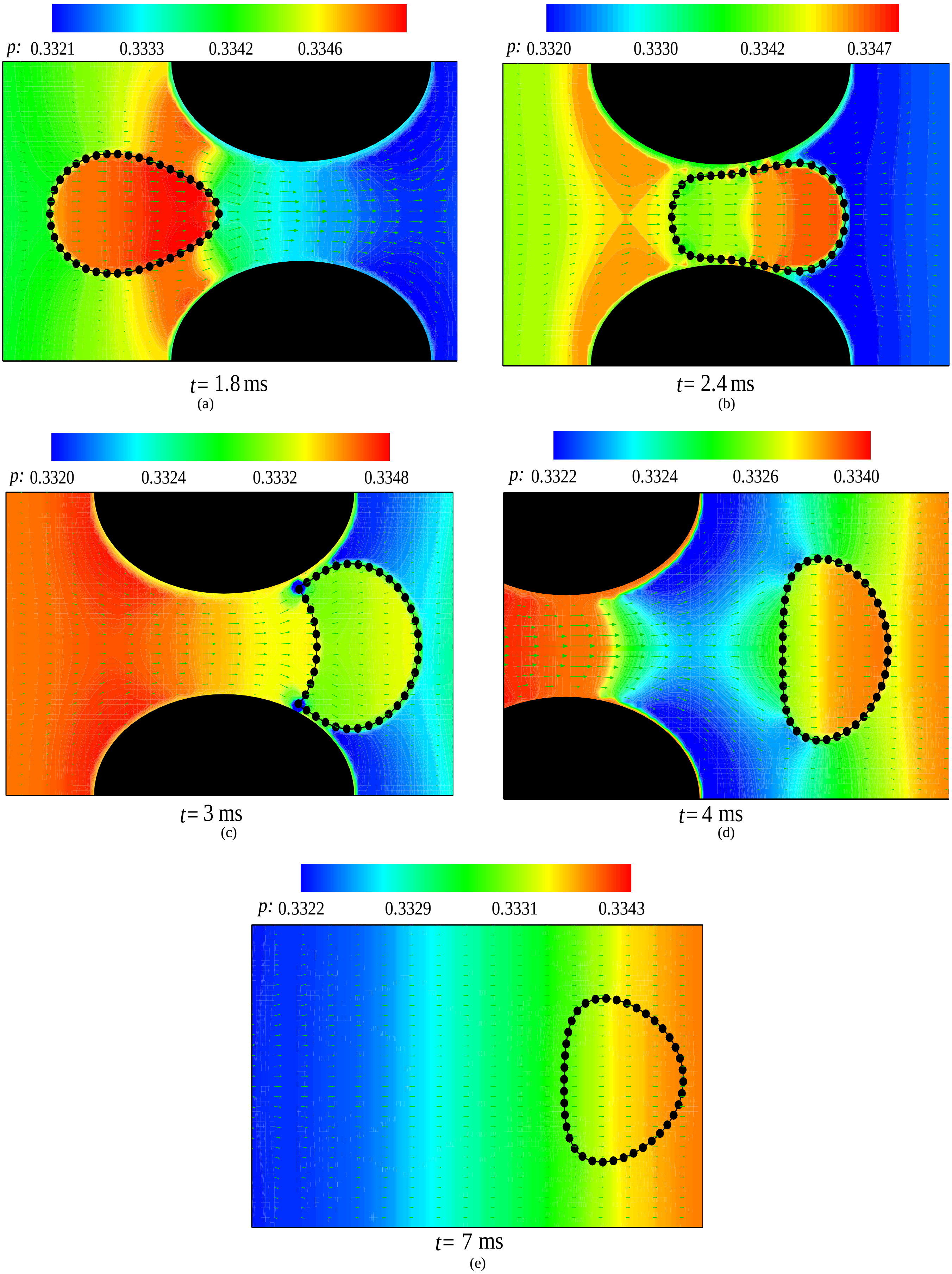


**Figure 4.** Motion of the body with a low flexibility passing stenosis at the times a) t = 1.8ms, b) t = 2.4ms, c) t = 3ms, d) t = 4ms and e) t = 7ms.

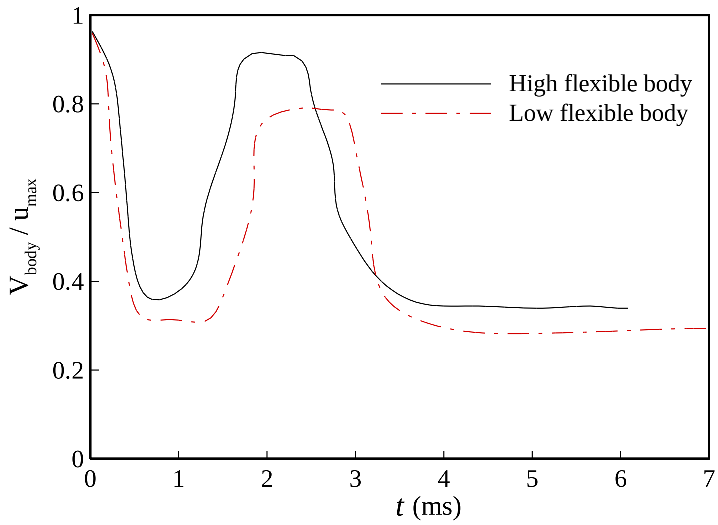


**Figure 5.** Comparison of velocity between high flexibility and low flexibility bodies.

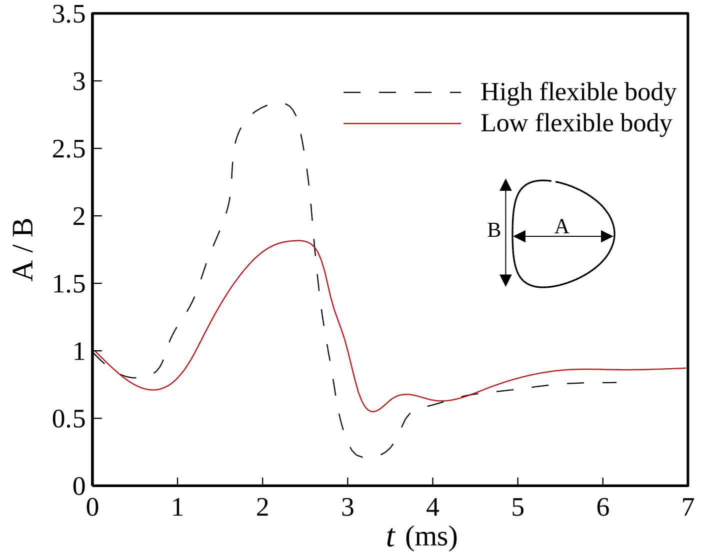


**Figure 6.** Comparison of A / B ratio of high elasticity body and low elasticity body

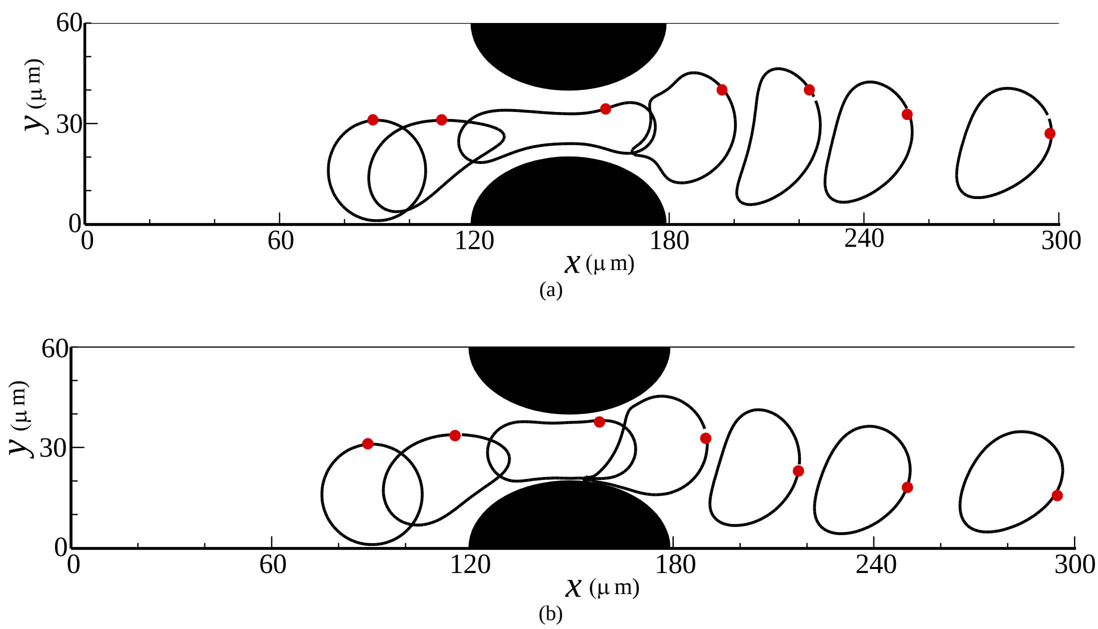


(a)

(b)

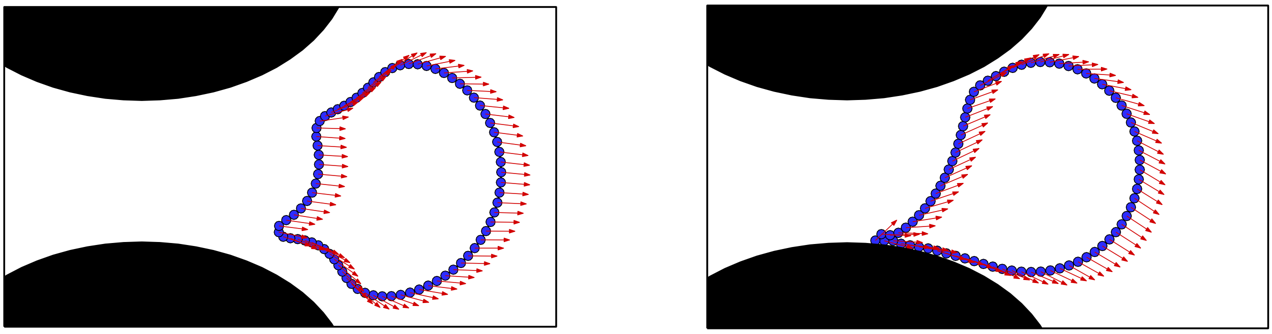

(c) (d)

**Figure 7.** a) Tank -treading motion of immersed body with high flexibility; b) Tank -treading motion of immersed body with low flexibility; c) Lagrangian points velocity vector of immersed body with high flexibility at the threshold of stenosis; and d) Lagrangian point velocity vector of immersed body with low flexibility at the threshold of stenosis

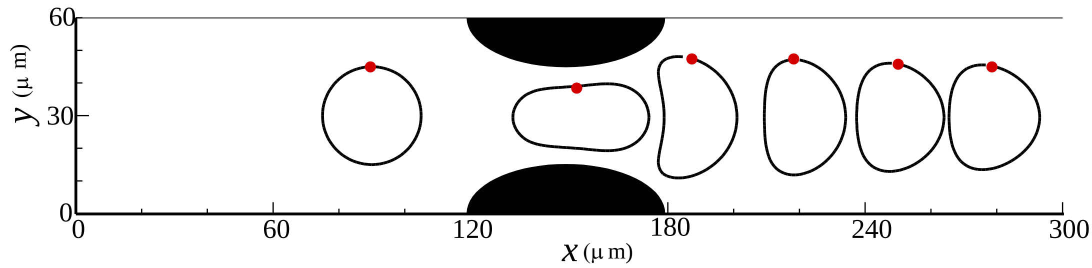


(a)

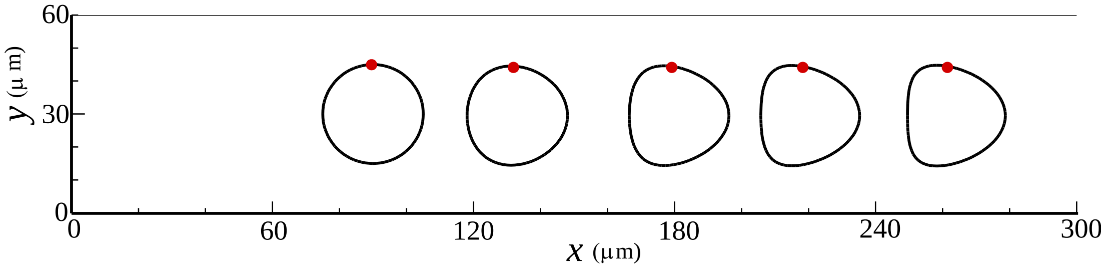


(b)

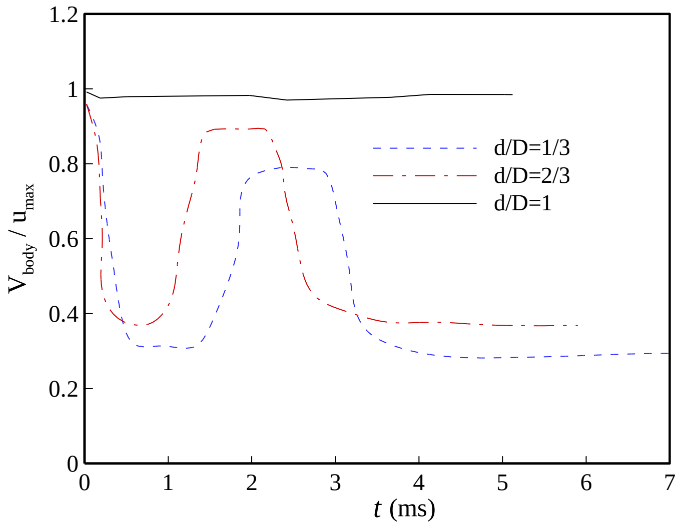


(c)

**Figure 8.** a) Deformation of body with low flexible for case d / D = 2/3, b) Deformation of body with low flexible for case without stenosis and d / D = 1, and c) comparison velocity for various sizes of stenosis.

**5. Acknowledgment**

The authors wish to thank the Ahvaz Branch, Islamic Azad University, Ahvaz, Iran, for the financial support.

**6. Appendix**

The used Nomenclature in the manuscript is as follow as

| | |
|---|---|
| $c$ | particle streaming speed |
| $\hat{e}_i$ | discrete particle speeds |
| $E_s$ | elastic modulus |
| $E_b$ | bending modulus |
| $f_i$ | density distribution function |
| $f^{eq}$ | equilibrium distribution function |
| $f$ | force density of the fluid |
| $L$ | Lagrangian force density |
| $S_i$ | external force |
| £ | elastic energy density |
| $N$ | total number of Lagrangian nodes |
| $s$ | Lagrangian coordinate |
| $u$ | fluid velocity |
| $U$ | body velocity |
| $X$ | position on the membrane |
| $x$ | Eulerian coordinate |
| $\rho$ | fluid density |
| $w_i$ | weight coefficients in direction i |
| $\tau$ | relaxation time |
| $\delta$ | delta function |
| $\Delta t$ | lattice time step |
| $\Delta x$ | lattice spacing |

**References**

1. Abbasszadeh Rad, A. and B. Vahidi, *A finite elements study on the role of primary cilia in sensing mechanical stimuli to cells by calculating their response to the fluid flow*. Journal of Computational Applied Mechanics, 2016. 47(1): p. 35-44.
2. Beigzadeh, B. and M. Halabian, *The effect of static magnetic field on hemodynamic properties of blood flow containing magnetic substances*. Journal of Computational Applied Mechanics, 2016. 47(2): p. 181-194.
3. Dastani, K., M. Moghimi Zand, and A. Hadi, *Dielectrophoretic effect of nonuniform electric fields on the protoplast cell*. Journal of Computational Applied Mechanics, 2017. 48(1): p. 1-14.
4. Tian, F., H. Luo, L. Zhu, J. Liao, and X. Lu, *An efficient immersed boundary-lattice Boltzmann method for the hydrodynamic interaction of elastic filaments*. Journal of computational physics, 2011. 230(19): p.7266-7283.
5. Wu, J.,and C. Shu, *Implicit velocity correction-based immersed boundary-lattice Boltzmann method and its applications*. Journal of Computational Physics, 2009. 228(6): p.1963-1979.
6. Peskin, C.S., *The immersed boundary method*. Acta numerica, 2002. 11: p. 479-517.
7. Mohamad, A.A., *Lattice Boltzmann method: fundamentals and engineering applications with computer codes*. 2011: Springer Science & Business Media.
8. Feng, Y., K. Han, and D. Owen, *Coupled lattice Boltzmann method and discrete element modelling of particle transport in turbulent fluid flows: Computational issues*. International Journal for Numerical Methods in Engineering, 2007. 72(9): p. 1111-1134.
9. Le, G. and J. Zhang, *Boundary slip from the immersed boundary lattice Boltzmann models*. Physical Review E, 2009. 79(2): p. 026701.
10. Dupuis, A., P. Chatelain, and P. Koumoutsakos, *An immersed boundary–lattice-Boltzmann method for the simulation of the flow past an impulsively started cylinder*. Journal of Computational Physics, 2008. 227(9): p. 4486-4498.
11. Wu, J. and C. Shu, *Implicit velocity correction-based immersed boundary-lattice Boltzmann method and its applications*. Journal of Computational Physics, 2009. 228(6): p. 1963-1979.
12. JiSeok, L. and L. SangHwan, *Flow around a flexible plate in a free stream*. Journal of Mechanical Science and Technology, 2011. 25(2): p. 379-390.
13. Zhang, J., P.C. Johnson, and A.S. Popel, *An immersed boundary lattice Boltzmann approach to simulate deformable liquid capsules and its application to microscopic blood flows*. Physical biology, 2007. 4(4): p. 285.
14. Zhang, J., P.C. Johnson, and A.S. Popel, *Red blood cell aggregation and dissociation in shear flows simulated by lattice Boltzmann method*. Journal of biomechanics, 2008. 41(1): p. 47-55.
15. Cheng, Y. and H. Zhang, *Immersed boundary method and lattice Boltzmann method coupled FSI simulation of mitral leaflet flow*. Computers & Fluids, 2010. 39(5): p. 871-881.
16. De Rosis, A. and E. Lévêque, *Central-moment lattice Boltzmann schemes with fixed and moving immersed boundaries*. Computers & Mathematics with Applications, 2016. 72(6): p. 1616-1628.
17. Habte, M.A. and C. Wu, *Particle sedimentation using hybrid Lattice Boltzmann-immersed boundary method scheme*. Powder Technology, 2017. 315: p. 486-498.
18. Coclite, A., et al., *A combined Lattice Boltzmann and Immersed Boundary approach for predicting the vascular transport of differently shaped particles*. Computers & Fluids, 2016. 136: p. 260-271.
19. Hu, Y., et al., *Immersed boundary-lattice Boltzmann simulation of natural convection in a square enclosure with a cylinder covered by porous layer*. International Journal of Heat and Mass Transfer, 2016. 92: p. 1166-1170.

20. Eshghinejadfard, A., et al., *Direct-forcing immersed boundary lattice Boltzmann simulation of particle/fluid interactions for spherical and non-spherical particles.* Particuology, 2016. 25: p. 93-103.
21. Li, Z. and J. Favier, *A non-staggered coupling of finite element and lattice Boltzmann methods via an immersed boundary scheme for fluid-structure interaction.* Computers & Fluids, 2017. 143: p. 90-102.
22. Pepona, M. and J. Favier, *A coupled Immersed Boundary–Lattice Boltzmann method for incompressible flows through moving porous media.* Journal of Computational Physics, 2016. 321: p. 1170-1184.
23. Revell, A., P. Mandal, and P. Day, *Application of a lattice Boltzmann-immersed boundary method for fluid-filament dynamics and flow sensing.* Journal of Biomechanics, 2016. 49(11): p. 2143-2151.
24. Sun, D.-K., et al., *A three-dimensional quantitative study on the hydrodynamic focusing of particles with the immersed boundary–Lattice Boltzmann method.* International Journal of Heat and Mass Transfer, 2016. 94: p. 306-315.
25. Wang, Y., et al., *An immersed boundary-lattice boltzmann flux solver in a moving frame to study three-dimensional freely falling rigid bodies.* Journal of Fluids and Structures, 2017. 68: p. 444-465.
26. Wu, J., et al., *GPU acceleration of FSI simulations by the immersed boundary-lattice Boltzmann coupling scheme.* Computers & Mathematics with Applications, 2016.
27. Liu, H., et al., *Lattice Boltzmann modeling of contact angle and its hysteresis in two-phase flow with large viscosity difference.* Physical Review E, 2015. 92(3): p. 033306.
28. Nash, R.W., et al., *Choice of boundary condition for lattice-Boltzmann simulation of moderate-Reynolds-number flow in complex domains.* Physical Review E, 2014. 89(2): p. 023303.
29. Afrouzi, H.H., et al., *Lattice Boltzmann analysis of micro-particles transport in pulsating obstructed channel flow.* Computers & Mathematics with Applications, 2015. 70(5): p. 1136-1151.
30. Bakhshan, Y. and A. Omidvar, *Calculation of friction coefficient and analysis of fluid flow in a stepped micro-channel for wide range of Knudsen number using Lattice Boltzmann (MRT) method.* Physica A: Statistical Mechanics and its Applications, 2015. 440: p. 161-175.
31. Rahimian, M.H. and R. Haghani, *Four different types of a single drop dripping down a hole under gravity by lattice Boltzmann method.* Journal of Computational Applied Mechanics, 2016. 47(1): p. 89-98.
32. Cao, C., et al., *Simulating the interactions of two freely settling spherical particles in Newtonian fluid using lattice-Boltzmann method.* Applied Mathematics and Computation, 2015. 250: p. 533-551.
33. Huang, J. and W.-A. Yong, *Boundary conditions of the lattice Boltzmann method for convection–diffusion equations.* Journal of Computational Physics, 2015. 300: p. 70-91.
34. Chen, L., et al., *Pore-scale study of diffusion–reaction processes involving dissolution and precipitation using the lattice Boltzmann method.* International Journal of Heat and Mass Transfer, 2014. 75: p. 483-496.
35. Sui, Y., et al., *Transient deformation of elastic capsules in shear flow: effect of membrane bending stiffness.* Physical Review E, 2007. 75(6): p. 066301.
36. Bouzidi, M.h., M. Firdaouss, and P. Lallemand, *Momentum transfer of a Boltzmann-lattice fluid with boundaries.* Physics of fluids, 2001. 13(11): p. 3452-3459.
37. Xiong, W. and J. Zhang, *Shear stress variation induced by red blood cell motion in microvessel.* Annals of biomedical engineering, 2010. 38(8): p. 2649-2659.
38. Ma, G., J. Hua, and H. Li, *Numerical modeling of the behavior of an elastic capsule in a microchannel flow: The initial motion.* Physical Review E, 2009. 79(4): p. 046710.
39. Fischer, T.M., M. Stohr-Lissen, and H. Schmid-Schonbein, *The red cell as a fluid droplet: tank tread-like motion of the human erythrocyte membrane in shear flow.* Science, 1978. 202(4370): p. 894-896.
40. Fischer, T. and H. Schmid-Schönbein, *Tank tread motion of red cell membranes in viscometric flow: behavior of intracellular and extracellular markers (with film)*, in *Red Cell Rheology*. 1978, Springer. p. 347-361.
41. Gaehtgens, P. and H. Schmid-Schönbein, *Mechanisms of dynamic flow adaptation of mammalian erythrocytes.* Naturwissenschaften, 1982. 69(6): p. 294-296.